

Remaining stress-state and strain-energy in tempered glass fragments

Nielsen, Jens Henrik

Published in:
Glass Structures & Engineering

Link to article, DOI:
[10.1007/s40940-016-0036-z](https://doi.org/10.1007/s40940-016-0036-z)

Publication date:
2016

Document Version
Publisher's PDF, also known as Version of record

[Link back to DTU Orbit](#)

Citation (APA):
Nielsen, J. H. (2016). Remaining stress-state and strain-energy in tempered glass fragments. Glass Structures & Engineering, 2(1), 45-56. DOI: 10.1007/s40940-016-0036-z

DTU Library

Technical Information Center of Denmark

General rights

Copyright and moral rights for the publications made accessible in the public portal are retained by the authors and/or other copyright owners and it is a condition of accessing publications that users recognise and abide by the legal requirements associated with these rights.

- Users may download and print one copy of any publication from the public portal for the purpose of private study or research.
- You may not further distribute the material or use it for any profit-making activity or commercial gain
- You may freely distribute the URL identifying the publication in the public portal

If you believe that this document breaches copyright please contact us providing details, and we will remove access to the work immediately and investigate your claim.

Remaining stress-state and strain-energy in tempered glass fragments

J. H. Nielsen

Received: 12 April 2016 / Accepted: 18 September 2016
© Springer International Publishing Switzerland 2016

Abstract When tempered glass breaks, it shatters into relatively small pieces depending on the residual stress state in the glass. This has been known for centuries and is currently used in standards for classifying whether a piece of glass is tempered or not. However, the process of fragmentation is complex and only a few, relatively simple, models have been suggested for predicting the fragment size. The full theoretical explanation is still to be found and this work aims at providing another brick to the puzzle. The strain-energy present in tempered glass is obviously contributing to the fragmentation process and some authors e.g. Barsom (J Am Ceram Soc 51(2):75, 1968), Gulati (Glass processing days, Tamglass Engineering Oy, Tampere, 1997), Warren (Fractography of glasses and ceramics IV, Alfred University, Alfred, 2001) and Tandon and Glass (Fracture mechanics of ceramics—active materials, nanoscale materials, composites, glass and fundamentals, Springer, Houston, 2005) have proposed models for the fragments size based on an energy approach. Often an estimate of the remaining strain energy in the fragment is used; which leaves the questions: (a) what parameters are important for the remaining strain energy? (b) what is the magnitude of the remaining strain energy? (c) is there a simple way to estimate the remaining strain energy?

The present paper applies a quasi-static finite element model in order to answer these questions. In the present paper an example on the deformation and the stress redistribution in a fragment is given. Furthermore, a parametric investigation on the strain energy remaining in cylindrical- and prismatic fragments is given. It is shown, that there exists a simple relation between the thickness of the glass pane and the remaining strain energy in the fragment. A simple method for estimating the remaining strain energy in a fragment of a given shape and initial residual stress state is presented.

Keywords Tempered glass · Fragments · Strain-energy · Residual stress · Fracture

1 Introduction

Glass is notoriously known for being a brittle material with a tensile strength governed by flaws in the surface. In tempered glass, the surface flaws are in compression, leading to a significant increase in apparent strength. This is one of the reasons why tempered glass is a popular material for many applications in the field of engineering. This surface compression is balanced by a tensile stress in the center part of the glass, the tensile zone, where only smaller and less critical flaws occur. These flaws, if any, in the central part are furthermore sealed from the surroundings and the strength is therefore time-independent and high enough to carry the relatively high permanent tensile stresses.

J. H. Nielsen (✉)
Technical University of Denmark, Brovej Building 118,
2800 Kgs. Lyngby, Denmark
e-mail: jhni@byg.dtu.dk

If the glass, for some reason, suddenly is unable to carry the tensile stresses in the center, the so-called fragmentation process will start. The fragmentation process is characteristic for tempered glass and leads to a failure, where the glass is fragmentized into small harmless pieces due, to release of the energy stored in the glass. The tempered glass is therefore sometimes referred to as safety glass.

This fragmentation process has fascinated people since the beginning of the 17th century where the so-called “prince rupert's drops”, “*Lacrymae Batavae*” or “Dutch tears” have been used for entertainment of the upper class since they are extremely strong in the bulk part. However, when the thin tail is broken, they fail completely into “dust” (very small fragments). These drops were investigated and reported by several authors e.g. [Hooke \(1665\)](#) in 1664 where he observed a relation between the cooling rate and the tendency to fragmentize. In 1877 a transcription of a French article is appearing in the [ScientificAmerican \(1877\)](#) where the increase in strength and the failure is explained by the residual stresses.

The small fragments in the above mentioned drops are caused by the high strain energy in the droplets, originating from the extremely rapid cooling. In tempered flat glass used today, the magnitude of the residual stresses is much lower and thereby the stored strain energy, is lower. As a result of this, the fragments in modern tempered flat glass are larger due to a lower cooling rate required for tempering flat glass without failure during the process. It seems therefore evident that a relation between the magnitude of residual stresses and the fragment size must exist. This has been investigated and proved experimentally by several authors ([Akeyoshi and Kanai 1965](#); [Barsom 1968](#); [Gulati 1997](#); [Schiavonato et al. 2005](#); [Mognato et al. 2011](#); [Lee et al. 2012](#); [Reich et al. 2013](#)). Several models for relating the fragment size to the residual stress state have been suggested in the literature, e.g. ([Barsom 1968](#); [Gulati 1997](#); [Shutov et al. 1998](#); [Warren 2001](#)) some of which incorporate the possibility of a remaining strain energy in the fragment. Then the question arises: what is then the strain energy left in a fragment?

Most of the work trying to establish an analytical model for this is considering the release of the so-called tension strain energy defined as the part of the strain energy coming from the tensile stresses alone. This is first suggested by [Barsom \(1968\)](#) where it is

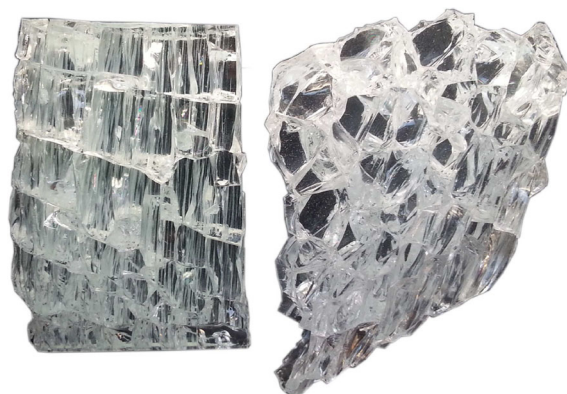


Fig. 1 Fragments, *left* float glass subjected to bending, *right* tempered glass (fragmentation initiated by diamond drill)

said that: “One of the many complications encountered is that the part of the stored elastic energy due to the compressive layers does not affect the fracture propagation as does that part due to the tensile region. This is verified by the fact that the fracture propagated in the tensile region first and then in the compressive layer over a period of time”. However, in more recent work, ([Nielsen et al. 2009](#); [Dugnani et al. 2014](#)) it is shown experimentally and analytically that the surface regions are cracking (almost) simultaneously with the center part. It is therefore decided, in the present work, to investigate the total strain energy in a fragment.

When tempered glass fails, energy is obviously released and the amount of energy available for driving the fragmentation process is not only dependent on the degree of tempering, but also on the method for initiating the failure. Bending of ordinary float glass may lead to a fracture pattern with small pieces due to the energy built-up during bending before failure, however, a closer look at the failure fragments will reveal a clear difference, see Fig. 1.

The fragmentation process can be initiated without practically adding energy to the glass. Some authors, ([Barsom 1968](#); [Nielsen et al. 2009](#)), have drilled with diamond tipped drills into the tensile zone, in order to minimize the energy added to the system. In these cases, it is reasonable to assume, that only the stored strain energy, from the residual stresses, are driving the fragmentation. In general the amount of energy available for driving the fragmentation, U_0 , can be written as:

$$U_0 = U_{\text{residual stress}} + U_{\text{loading}} \quad (1)$$

where it should be noted that in this study, it is assumed that the glass is not loaded, leading to $U_0 = U_{\text{residual stress}}$.

When the glass fragmentizes, energy is used for creating new surfaces (cracking), kinematics and deformation (heat). The strain energy left in a fragment, U_1 , must therefore be given as:

$$U_1 = U_0 - U_{\text{surface}} - U_{\text{kinetic}} - U_{\text{heat}} - U_{\text{other}} \quad (2)$$

where U_{other} represents other energy consuming effects such as sound. In this study, only the difference between the final energy state and the initial energy state is considered, leaving the terms in U_1 (except for U_0) to be unknown.

In order to use an energy criterion for setting up a valid theory, predicting the fragmentation process in tempered glass, it is necessary to have knowledge of the energy left in the fragment after fragmentation. If we consider a single fragment, there will obviously be a reduction in the stresses when it is fragmentized and thereby a reduction in strain energy. This paper investigated the change of stress state in a fragment which is important in order to develop a theory capable of explaining the relation between fragments size, thickness and residual stress. In other words; the present work aims at determining U_1 in (2).

2 Deriving the initial strain energy, U_0 , in a cylindrical fragment

It is common to assume that the equilibrated stress state, σ , through the thickness of a (thin) glass plate is planar hydrostatic (equal in the plate plane and zero in the transverse direction) and distributed parabolic over the thickness. This assumption is reasonable as long as only locations far from edges are considered. Figure 2 is showing the residual stress distribution over the thickness, far from an edge. The zero stress contour line, separating the tensile zone and the compression zone is also sketched. This parabolic stress distribution, $\sigma(z)$, can be written in terms of the surface stress, σ_s , as:

$$\sigma(z) = \sigma_s \frac{1}{2} (1 - 3\xi^2), \quad \xi = \frac{2z}{h} \quad (3)$$

using symbols defined in Fig. 2. From the parabolic stress distribution, which is in equilibrium and sym-

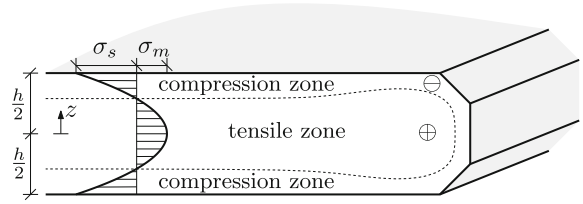


Fig. 2 Stress distribution far away from edges and a sketch showing a contour line at zero stress

metric about the mid-plane, it is easy to derive the well-known rule of thumb saying that the compressive surface stress is twice the tensile stress in magnitude, $2\sigma_m = -\sigma_s$, and that the zero stress contour line is located at a depth of approximately 21 % of the thickness, h .

The strain energy in a fragment before the glass actually fragmentizes can be calculated analytically. This has been done by several authors for fragments with a box shape (rectangular parallelepiped), in the following it will be done for a cylindrical fragment which is used as a reference value here. However, the strain energy per surface area will obviously be the same as found by other authors.

The strain energy for a fragment in tempered glass (assumed linear elastic) before fragmentation, U_0 , can be written as:

$$U_0 = \frac{1}{2} \int_V \sigma_{ij} \varepsilon_{ij} dV = \frac{1}{2} \int_V (\sigma_r \varepsilon_r + \sigma_\theta \varepsilon_\theta) dV \quad (4)$$

where V is the domain (volume) of the fragment considered, σ_{ij} and ε_{ij} are the stress- and strain tensor respectively. The factor of $\frac{1}{2}$ is due to the assumption of the linear elastic material behaviour. The second equal sign due to the before mentioned assumption of a planar hydrostatic stress state where the only non-zero stresses are $\sigma = \sigma_r = \sigma_\theta \neq 0$. Applying Hooke's law in cylindrical coordinates, we obtain:

$$U_0 = \frac{1-\nu}{E} \int_V \sigma^2 dV \quad (5)$$

Inserting the residual stress field from (3) and integrating over the cylinder we find:

$$\begin{aligned} U_0 &= \frac{1-\nu}{E} \int_{z=-h/2}^{z=h/2} \int_{r=0}^{r=R} \int_{\theta=0}^{\theta=2\pi} \sigma^2 r d\theta dr dz \\ &= \frac{h\pi R^2(1-\nu)}{5E} \sigma_s^2 \end{aligned} \quad (6)$$

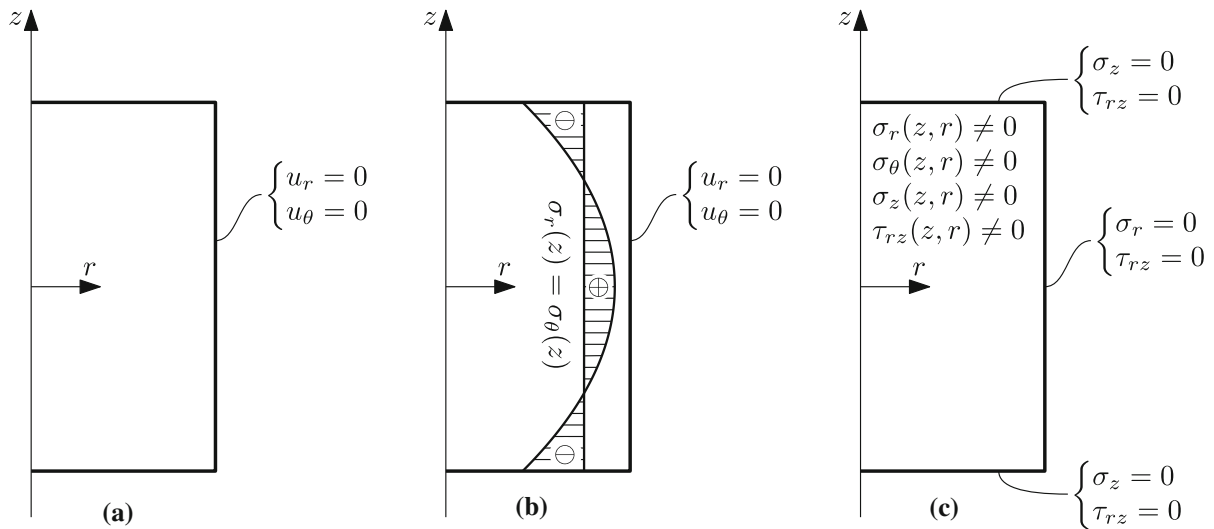


Fig. 3 Axisymmetric model of the cylindrical fragment in three steps. The z -axis is used as the rotational axis. **a** Initial stress free step, **b** residual stress state is applied by means of a temperature

distribution, **c** boundary condition on the free vertical edge is removed. Due to superposition, the residual stress state can be applied directly on **c**

which is the initially stored strain energy in a cylindrical fragment of radius, R , height, h , and with an initial residual surface stress of σ_s .

Dividing with the base area for the cylinder we obtain the strain energy per unit surface area of any given base shape of the fragment:

$$U_0 = \frac{h(1-\nu)}{5E} \sigma_s^2 \quad (7)$$

Which is in line with what is found in the literature, (Barsom 1968; Gulati 1997; Warren 2001; Reich et al. 2012).

3 The remaining strain energy in a fragment: U_1

This section investigates the remaining energy in a fragment after the fragmentation, U_1 . This investigation is carried out by means of a finite element model of the problem. The (quasi)static response is searched for and an implicit code is therefore used in order to minimize computational time.

In general the initial residual stress state is applied by means of a temperature variation over the height of the fragment, $T(z)$, which is related to the stress distribution in the following way:

$$\sigma(z) = \frac{\alpha E}{1-\nu} \Delta T(z) \quad (8)$$

where α , E and ν are the thermal expansion, Youngs modulus and Poisson's ratio respectively. $\Delta T(z)$ represents the temperature variation, which is a function of the coordinate z . Applying a temperature distribution, $T(z)$, having the same shape as the equilibrated stress state given by (3) will allow us to represent the unbroken glass pane by supporting the vertical boundary from any in-plane movements as shown in Fig. 3b. Next step; the boundary conditions on the vertical edge are removed in order to simulate the free edge of the fragment, see Fig. 3c. Due to the linear nature of the problem (small deformations and linear elastic material behaviour) it is sufficient just to apply the stress state described by (8) on a model with the boundary conditions shown in Fig. 3c. This procedure is used in the following.

3.1 Cylindrical fragment

For the cylindrical fragment, the model is created in the finite element program ABAQUS v. 6.14-2 using CAX8 elements which are eight node axi-symmetric displacement elements. Due to the symmetric nature of the problem, the $r\theta$ -plane is utilized for symmetry

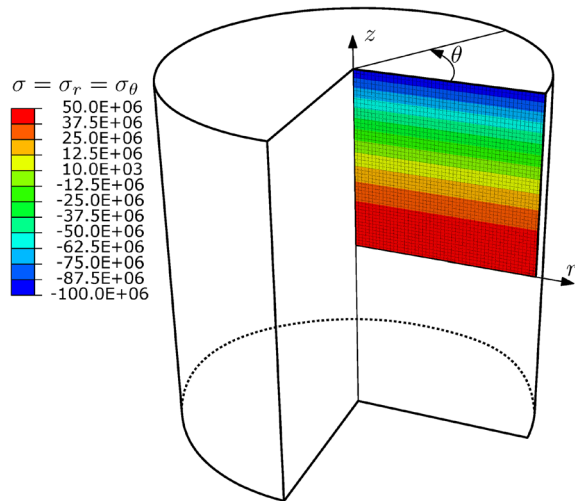


Fig. 4 Axisymmetric model of the cylindrical fragment

as indicated in Fig. 4. A convergence analysis have been performed for the calculations and relatively few elements are needed in order to capture the strain energy, however, it is chosen for the axisymmetric model to apply smallest element size according to either having 30 elements along the radius or 50 elements over half the height. The elements are always kept strictly rectangular and with a side ratio as close as possible to one.

Before fragmentation the stress state is planar hydrostatic, however, when the fragment is formed this changes and the stress state in the fragment becomes fully three dimensional. In case of the cylindrical fragment, the four different axi-symmetric stresses are shown in Fig. 5, and it is seen that stresses in the thickness direction becomes significant. Actually, the largest principal stress for this fragment is located in the center with a transverse direction (σ_z). It can also be seen that the shear stress becomes significant and that the radial and tangential stresses are very similar in magnitude and distribution, but not equal.

Apart from showing the stresses, Fig. 5 is also illustrating the deformations in a fragment, however, it should be noticed that the deformations are magnified 100 times and the measures given are only valid for this particular fragment size and initial stress distribution.

4 Results and discussion

The amount of strain energy remaining in a fragment with a high stress state is obviously higher than in a

fragment with a lower stress state. If we consider the strain energy left in a fragment relative to the strain energy in the same area before fragmentation, U_{RR} , as given in (9), it will be independent on the initial stress state due to the linear nature of the problem.

For that reason, the results are presented by the relative remaining strain energy, U_{RR} :

$$U_{RR} = \frac{U_1}{U_0} \quad (9)$$

which must be in the interval: $0 < U_{RR} < 1$.

4.1 Variation with the fragment size

The remaining strain energy in a fragment, U_1 , is dependent on the size of the fragment and so is the U_{RR} as shown in Fig. 6 where the variation with the fragment surface area¹, A , and the thickness, h , is shown. From the figure it is seen that U_{RR} is approaching 1 as the fragment size is increased which is as expected. It is also seen, that in a fragment from a thick plate the relative remaining strain energy is less than in a thin fragment which is expected due to relatively more slender geometry.

From Fig. 6 it is seen that curves for the different thicknesses have the same shape. If the abscissa is normalized by h^2 it turns out that all the curves can be brought to coincide as shown in Fig. 7.

From Fig. 7 it is seen that U_{RR} is only dependent on the ratio of A/h^2 . In the following the measure A/h^2 is therefore used.

4.2 Stresses in the cylindrical fragment

Like the strain energy, the stress state is dependent on the measure A/h^2 and the magnitude is scaled with the initial residual stress state. In Figs. 8, 9, 10 and 11 the four different stress components are shown for five different values of A/h^2 representing the maximum fragment size for different thicknesses according to Eurocode (EN12150 2004), see Table 1. Only the symmetric part of the fragment is given in the figures. The element mesh is not shown in the figures in order to have a clear plot, however, the mesh density is as described earlier.

¹ The fragment surface area is the area of the base shape of the fragment (fragment volume divided by thickness).

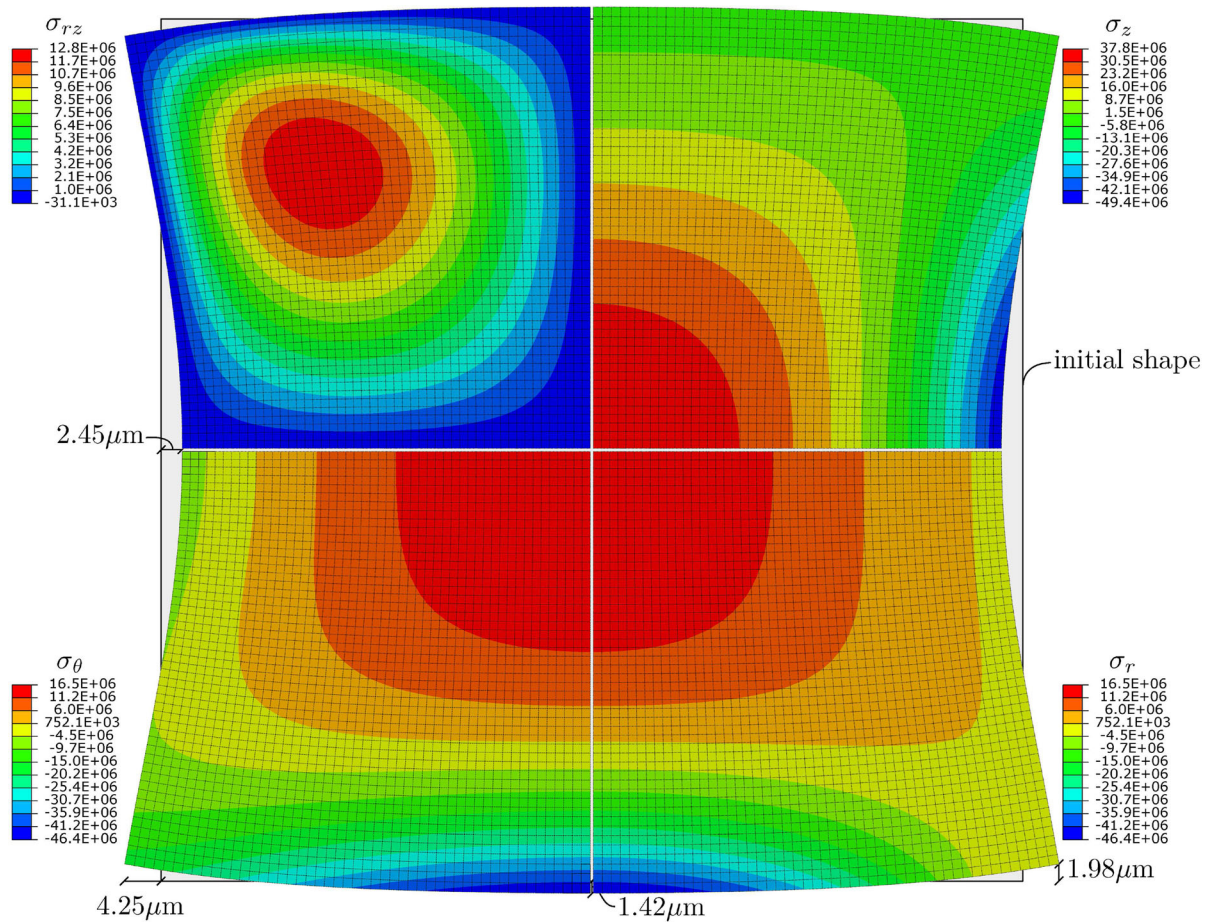


Fig. 5 Stress state in a cylindrical fragment from, total height is 10 mm, and the diameter is also 10 mm. The initial stress state is parabolic with a surface stress of -100 MPa as shown in Fig. 3.

The grey area in the central part of the large fragment in Fig. 8, indicates that the tangential stress, σ_θ , is slightly higher than 50 MPa which is an increase compared to the initial stress. The same is observed for the radial stresses, σ_r , in Fig. 9.

For both tangential and radial stresses a decreases with the fragment size, as expected is seen, see Figs. 8 and 9. The small fragments, corresponding to the maximum size for fully tempered 15 mm glass ($A/h^2 = 0.37$), are nearly stress free as also indicated in Table 1 where it is seen that only about 5 % of the initial strain energy remains in the fragment.

The tangential stresses are generally higher than the radial due to the cylindrical shape of the fragment. For the tangential stresses, it is seen that the variation is nearly undisturbed at a distance of approximately $3/4h$,

Note that the undeformed fragment is shown behind the contour plot and the displacements are given in selected points

from the edge. For the radial stresses the same distance is approximately equal to h .

For the longitudinal stresses or through-thickness stress, σ_z , of the fragment, it should be remembered that this component initially is zero; however, after fragmentation relatively high longitudinal stresses are found. Looking at Fig. 10, it is seen that the maximum stress is found in a medium size fragment whereas the minimum stress is found in the largest fragment. This indicates that there is a fragment size at which the maximum longitudinal stress is maximum. From Fig. 12 this maximum is seen to be for $A/h^2 = 0.94$.

Again Saint-Venant's principle hold since the longitudinal stress state is not affected by the free edge more than one to two heights from the edge.

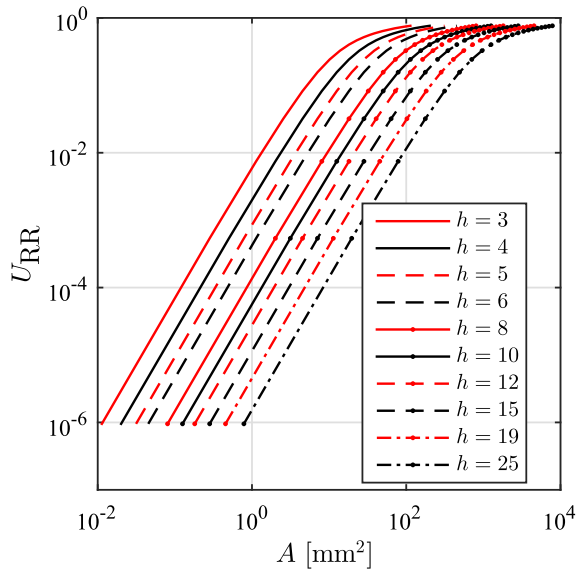


Fig. 6 Showing the relative remaining strain energy in a cylindrical fragment as a function of the fragment surface area, A , for different thicknesses, h

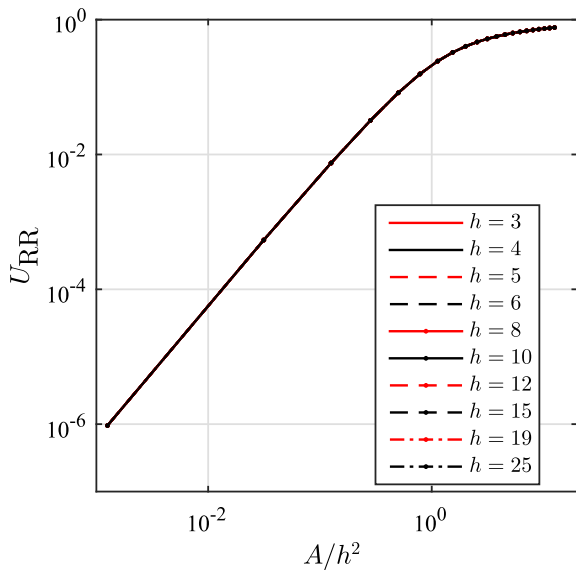


Fig. 7 Showing the relative remaining strain energy in a cylindrical fragment as a function of the fragment size given by A/h^2 . Note that all curves are coinciding

For the completeness, the last stress component, namely the shear stress, is shown in Fig. 11. Again it is seen that the maximum shear stress is not found in the largest nor the smallest fragment and the stress state is only affected at a distance of one to two heights from the free edge.

It is interesting to notice in Fig. 12 that in general the extreme stress values are decreasing with the fragment size, except for the through-thickness stress, σ_z , which have a maximum value of approximately 40 MPa for $A/h^2 = 0.94$. It should be noted that $\max(\sigma_r) \approx \max(\sigma_\theta)$, $\min(\sigma_r) \approx \min(\sigma_\theta)$ and $\min(\sigma_{rz}) = 0$.

4.3 Polygon fragment shape

The cylindrically shaped fragment is obviously a simplified geometry used for modelling, but how realistic is it? It is clear that the shape of the fragments never will be perfectly cylindrical; however, it is a common assumption to use prisms with a regular polygonal shaped based for the fragments even thou this is also a simplified approach. In the literature the rectangular prisms and the hexagonal prisms are the ones most often assumed. Experimentally, we see quite a variety of shapes, so investigating different shapes will be of interest. In this study, different regular polygonal shapes as shown in Fig. 13 will be investigated for varying size.

The FE models for the polygonal prisms are very similar to what is described for the axi-symmetric model; however, the used elements are so-called wedge elements with mid-side nodes (C3D15). For the 3D models the high degree of symmetry is used which means that only $\frac{1}{2n}$ of the base polygon is modelled and only half the height, so e.g. for the hexagon only $\frac{1}{24}$ of the geometry is modelled. Convergence in the results are easily found. As an example, a model of a fragment with four sides ($n = 4$) and a $A/h^2 = 1.05$ is modelled with both 3164 (standard configuration) elements and 420 elements and it was found that the difference in U_{RR} was about 0.16 %.

From Fig. 14 it is seen that for fragments with $n > 5$ the assumption of a cylindrical fragment is reasonable. In order to investigate this further, a plot showing the deviation of the relative remaining strain energy from a cylindrical fragment (having the same base area), as a function of the number of sides in the regular polygon forming the base of the fragment is given in Fig. 15. From this figure it is seen, as expected, that the triangular shape is the worst. It is also seen that this tendency seem to diminish for larger fragments. From the Figure it is also seen that the large fragments approaches the $n = \infty$ value from below whereas the small fragments approaches from above. This could be explained by the

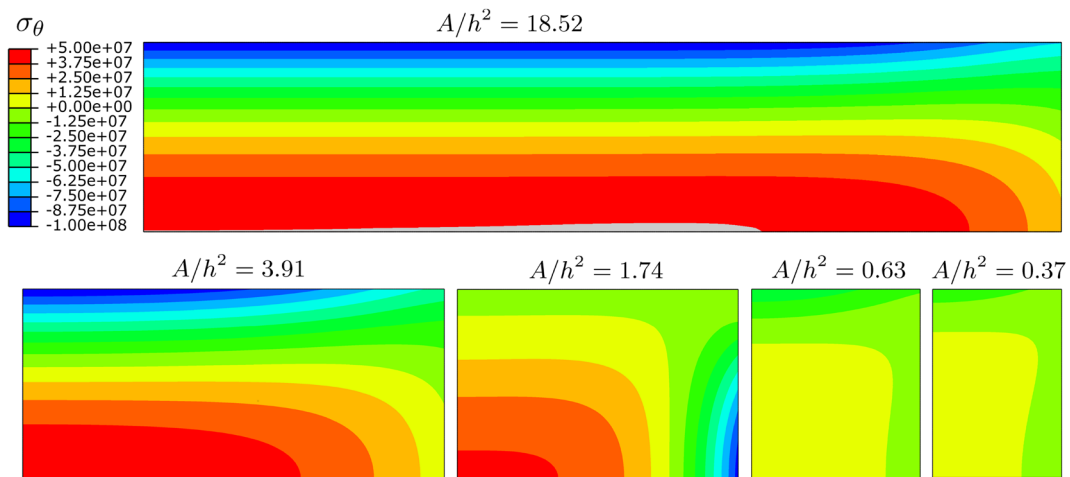


Fig. 8 Tangential stress state (σ_θ) in cylindrical fragments of varying size. Only half the height, h , and half the diameter is shown

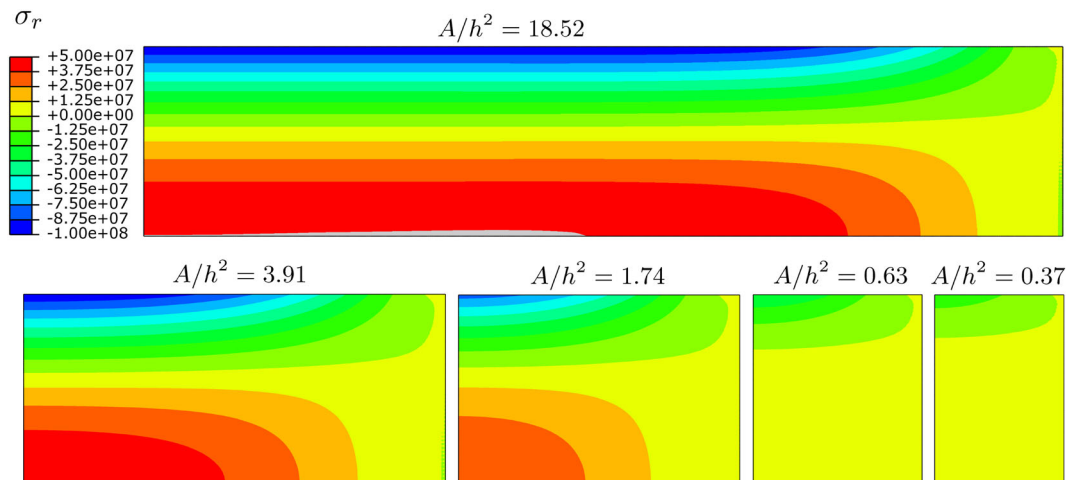


Fig. 9 Radial stress state (σ_r) in cylindrical fragments of varying size. Only half the height, h , and half the diameter is shown

complex redistribution of stresses in the fragments as showed in Sect. 4.2.

Considering the minimum particle counts on a 50 mm × 50 mm square, N_{50} , given in EN12150 (2004), realistic maximum values for A/h^2 in fully tempered glass for different thicknesses are given in Table 1.

A reasonable range covering also smaller fragments could therefore be $0.1 < A/h^2 < 20$.

Relevant parts of the plot given in Fig. 14 have been tabulated in Table 2.

Due to the almost straight line in the log-log plot in Fig. 14 for low values of A/h^2 it is recommended to use a logarithmic interpolation in Table 2. If the value, $y(x)$, between two points (x_1, y_1) and (x_2, y_2) in Table 2

is wanted, the following interpolation formula can be used:

$$y(x) = y_1 \left(\frac{x}{x_1} \right)^b, \quad \text{where } b = \frac{\log y_2 - \log y_1}{\log x_2 - \log x_1} \quad (10)$$

5 Example

The residual stress in a 19 mm thick specimen made of tempered glass is measured to be 130 MPa. A fragmentation test results in an average surface area of each fragment of $A = 70 \text{ mm}^2$. Assuming square fragments

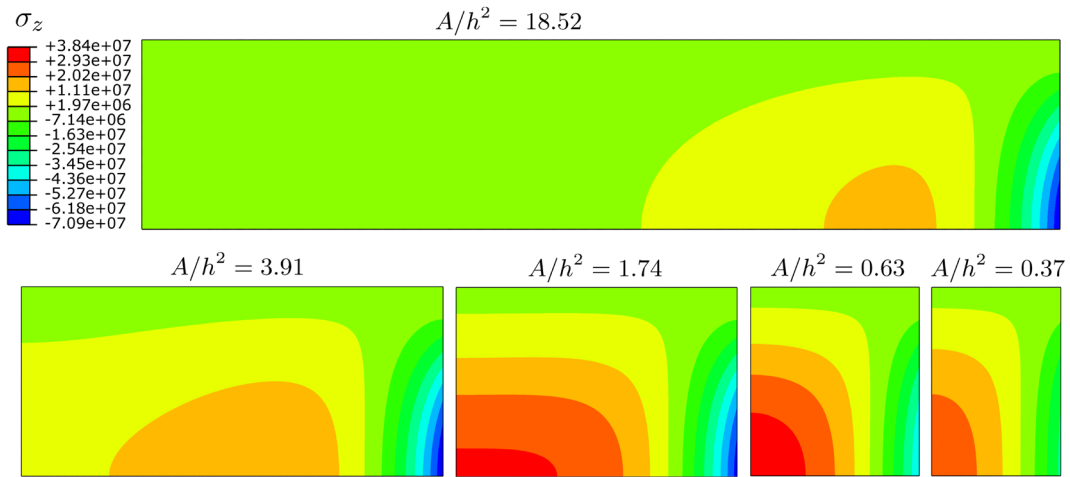


Fig. 10 Longitudinal stress state (σ_z) in cylindrical fragments of varying size. Only half the height, h , and half the diameter is shown

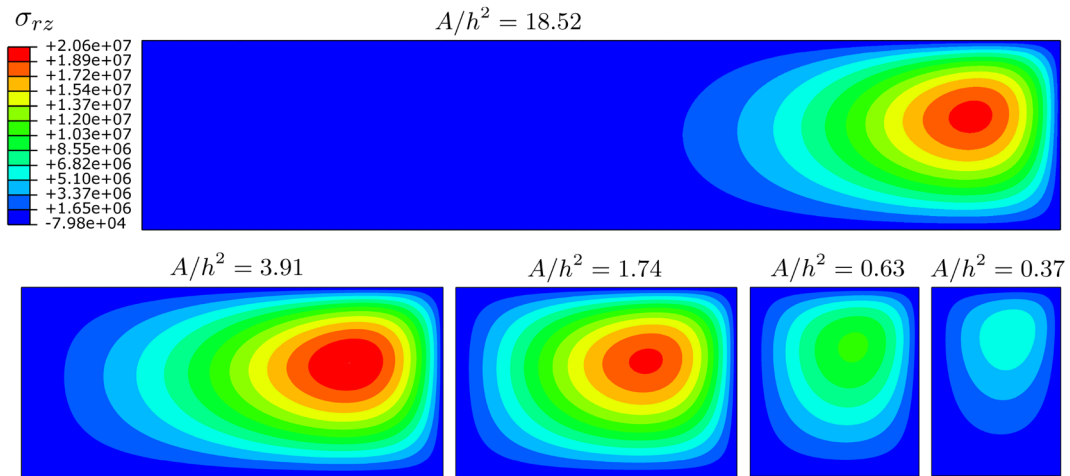


Fig. 11 Shear stress state (σ_{rz}) in cylindrical fragments of varying size. Only half the height, h , and half the diameter is shown

($n = 4$) the initial strain energy, U_0 , and the remaining strain energy, U_1 , can be estimated.

The initial strain energy is found from (7) multiplying with the area, A :

$$U_0 = 70 \times 10^{-6} \frac{19 \times 10^{-3}(1-0.23)}{5.70 \times 10^9} (130 \times 10^6)^2 \text{ J} \\ = 49.45 \times 10^{-3} \text{ J} \quad (11)$$

the size of the fragment is: $A/h^2 = 0.194$ which can be used for interpolating in Table 2 according to (10):

$$b = \frac{\log 0.032 - \log 0.002}{\log 0.25 - \log 0.05} = 1.723 \quad (12)$$

Now the relative remaining strain energy for $A/h^2 = 0.194$ can be found:

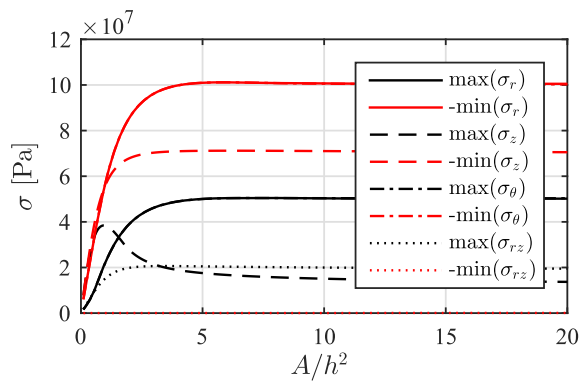
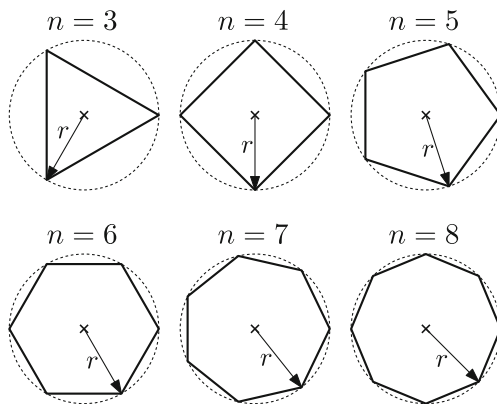
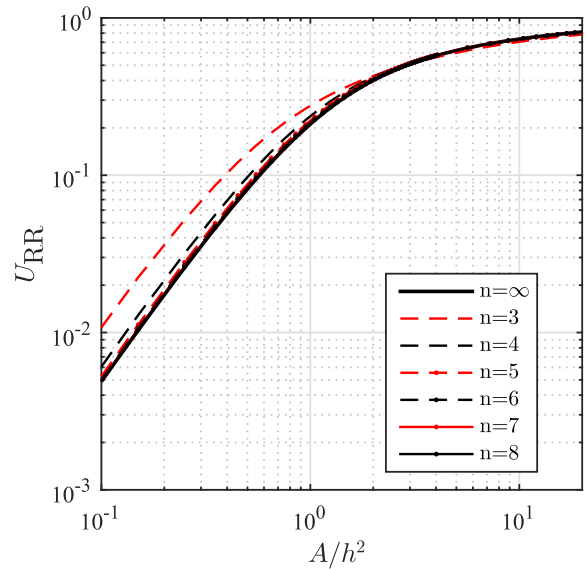
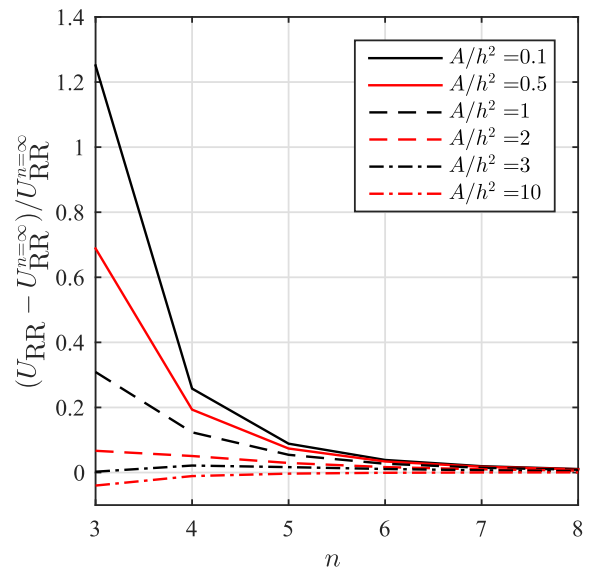
$$U_{RR} = 0.002 \left(\frac{0.194}{0.05} \right)^{1.723} = 0.021 \quad (13)$$

From this the remaining strain energy, U_1 , can be calculated by (9):

$$U_1 = 0.021 \cdot 49.45 \times 10^{-3} \text{ J} = 1.022 \times 10^{-3} \text{ J} \quad (14)$$

Table 1 Realistic maximum values for A/h^2 derived from Eurocode (EN12150 2004)

h (mm)	N_{50} (-)	A (mm ²)	A/h^2 (-)	U_{RR} (-)
3	15	166.7	18.52	0.807
4	40	62.5	3.91	0.569
5	40	62.5	2.50	0.461
6	40	62.5	1.74	0.361
8	40	62.5	0.98	0.206
10	40	62.5	0.63	0.115
12	40	62.5	0.43	0.064
15	30	83.3	0.37	0.050
19	30	83.3	0.23	0.022

**Fig. 12** The maximum and minimum remaining stress in a fragment as a function of the size. The initially stress state was -100 MPa surface compression (σ_s) and 50 MPa tensile center stress (σ_m). Note that the minimum stresses are multiplied by -1 **Fig. 13** Parametric study, the range of regular polygonal shapes investigated in addition to the cylindrical fragment**Fig. 14** Relative remaining strain energy as a function of the fragment sizes for different (n)-regular polygon shaped fragments. Note that Table 2 provides a tabulated form of the data**Fig. 15** Deviation from a cylindrical fragment keeping a constant surface area, A , but with varying base geometry

This result is deviating with 1.2% from a FEM calculation; however, if linear interpolation for finding U_{RR} had been used, a 15% deviation would have been found.

Table 2 Tabular data for the relative remaining strain energy, U_{RR} , in fragments of different polygonal shapes. For $n > 5$ the column for $n = \infty$ will provide reasonable results with a largest relative deviation of less than 4 % in the table

A/h^2	$n = 3$	$n = 4$	$n = 5$	$n = \infty$
0.05	0.003	0.002	0.001	0.001
0.25	0.052	0.032	0.028	0.026
0.45	0.121	0.083	0.074	0.069
0.65	0.186	0.141	0.129	0.121
0.85	0.241	0.198	0.184	0.173
1.05	0.287	0.250	0.235	0.223
1.25	0.326	0.295	0.281	0.269
1.45	0.358	0.335	0.323	0.310
1.65	0.386	0.370	0.359	0.346
1.85	0.411	0.401	0.391	0.379
2.05	0.432	0.427	0.419	0.407
2.25	0.452	0.451	0.444	0.433
2.45	0.469	0.472	0.466	0.456
2.65	0.485	0.490	0.486	0.476
2.85	0.499	0.507	0.504	0.495
3.05	0.512	0.522	0.520	0.512
3.25	0.524	0.536	0.535	0.527
3.45	0.535	0.549	0.548	0.541
3.65	0.546	0.560	0.560	0.554
3.85	0.556	0.571	0.572	0.566
4.05	0.565	0.581	0.582	0.577
5.65	0.621	0.642	0.645	0.643
7.25	0.660	0.681	0.686	0.686
8.85	0.688	0.710	0.715	0.717
10.45	0.711	0.732	0.738	0.740
12.05	0.729	0.750	0.755	0.759
13.65	0.744	0.764	0.770	0.774
15.25	0.756	0.776	0.782	0.786
16.85	0.767	0.787	0.793	0.797
18.45	0.777	0.796	0.802	0.806

6 Conclusion

The shattering, or fragmentation of tempered glass is an empirically well-known phenomenon which is used in daily engineering when e.g. characterizing tempered glass. This paper contributes to a further development of models capable to predict, on theoretic basis, the relation between residual stresses and fragment size. It is shown that parameters such as fragment size and initial residual stresses can be handled simply by scal-

ing the results. Looking at the expression for the strain energy before failure it is seen that these parameters are included in the remaining strain energy in a similar way. The geometry of the fragment could not be accounted for in a simple manner, however, a table covering polygon shapes have been provided.

In the literature it is a common assumption that a given part of the strain energy originating from tensile stresses are contributing to the fragmentation. This is also discussed and it is suggested, on the basis of more recent work, that using the full strain energy might be more reasonable.

From the investigation on the stress state in the cylindrical fragment it is found that:

1. The stress state changes from initially being planar hydrostatic ($\sigma_z = \sigma_{rz} = 0$) in the tempered glass to becoming fully tri-axial in the fragment.
2. The through-thickness stress component, σ_z , and the shear stress, σ_{rz} which initially are zero can be of a magnitude up to approximately 80 and 40 % of the initial residual tensile center stress, σ_m , respectively.
3. The maximum value for the through-thickness stress, σ_z , is found in a fragment with $A/h^2 = 0.94$.
4. Saint-Venant's principle holds and fragments having a radius of slightly above the thickness, h , or higher will have a central stress state which is nearly identical to the initial stress state.

Acknowledgments The author acknowledges Associate Professor John Forbes Olesen for discussing the results. However, J. F. Olesen should not be held responsible for any errors or wrong conclusions in the paper, these are the responsibility of the author alone.

References

- Akeyoshi, K., Kanai, E.: VII international congress on glass. (1965)
- Barsom, J.M.: Fracture of tempered glass. J. Am. Ceram. Soc. **51**(2), 75 (1968). doi:[10.1111/j.1151-2916.1968.tb11840.x](https://doi.org/10.1111/j.1151-2916.1968.tb11840.x)
- Dugnani, R., Zednik, R.J., Verghese, P.: Int. J. Fract. **190**(1-2), 75 (2014). doi:[10.1007/s10704-014-9975-z](https://doi.org/10.1007/s10704-014-9975-z). <http://link.springer.com/10.1007/s10704-014-9975-z>
- EN12150-2: Glass in Building—Thermally Toughened Soda Lime Silicate Safety Glass—Part 2: Evaluation of Conformity/Product Standard. (2004)
- Gulati, S.T.: Glass Processing Days. Tamglass Engineering Oy, Tampere (1997)
- Hooke, R.: Micrographia: Or, Some Physiological Descriptions of Minute Bodies Made by Magnifying Glasses. J. Martyn and J. Allestry, London (1665)

- Lee, H., Cho, S., Yoon, K., Lee, J.: Glass thickness and fragmentation behavior in stressed glasses. *N. J. Glass Ceram.* **02**(04), 116 (2012). doi:[10.4236/njgc.2012.24020](https://doi.org/10.4236/njgc.2012.24020)
- Mognato, E., Barbieri, A., Schiavonato, M., Pace, M.: In: *Glass Performance Days Proceedings*, pp. 115–118. (2011)
- Nielsen, J.H., Olesen, J.F., Stang, H.: *Exp. Mech.* **49**(6), 855 (2009). doi:[10.1007/s11340-008-9200-y](https://doi.org/10.1007/s11340-008-9200-y). <http://link.springer.com/10.1007/s11340-008-9200-y>
- Reich, S., Weller, B., Dietrich, N., Pfefferkorn, S.: Challenging glass 3: conference on architectural and structural applications of glass, CGC 2012 (June), 509. (2012)
- Reich, S., Dietrich, N., Pfefferkorn, S., Weller, B.: Elastic strain energy of thermally tempered glass increases its residual strength. In: *Glass Performance Days*, June 2013, pp. 348–352. (2013)
- Schiavonato, M., Mognato, E., Redner, A.S.: In: *Glass Processing Days*, pp. 1–4. (2005)
- ScientificAmerican*: Tempered glass. (1877). doi:[10.1038/scientificamerican01131877-18](https://doi.org/10.1038/scientificamerican01131877-18)
- Shutov, A.I., Popov, P.B., Bubeev, A.B.: Prediction of the character of tempered glass fracture. *Glass Ceram.* **55**(1–2), 8 (1998). doi:[10.1007/BF03180135](https://doi.org/10.1007/BF03180135)
- Tandon, R., Glass, S.J.: Controlling the fragmentation behavior of stressed glass. In: Bradt, R.C., Munz, D., Sakai, M., White, K.W. (eds.) *Fracture Mechanics of Ceramics—Active Materials, Nanoscale Materials, Composites, Glass and Fundamentals*. Springer, Houston (2005)
- Warren, P.D.: Effective volume and effective area for a ceramic C-ring test specimen. In: Varner, J.R., Quinn, G.D. (eds.) *Fractography of Glasses and Ceramics IV*, pp. 389–402. Alfred University, Alfred (2001)